Investigation of the M13 Globular Cluster: Characteristics and Pulsation Periods of Its RR Lyrae Stars V8, V31, and V54

Daniel Vurgaftman
Katherine Lee
Stanford Online High School, 415 Broadway Academy Hall, Floor 2, 8853, Redwood City, CA 94063; danyavur@gmail.com, kalee7798@gmail.com. There are two corresponding authors in this study; contributions of the first two authors were equal.

Jett Peters
Justin Wang
Kalėe Tock
Stanford Online High School, 415 Broadway Academy Hall, Floor 2, 8853, Redwood City, CA 94063; jettpeters2@gmail.com, justinw16688@gmail.com, kaleeg@stanford.edu

Received May 26, 2023; revised October 17, December 21, 2023, January 2, 2024; accepted January 13, 2024

Abstract Images of the Messier 13 (M13/NGC 6205) globular cluster were requested from the Las Cumbres Global Observatory's 40-centimeter telescope to investigate the chemical composition and characteristics of the cluster along with three of its RR Lyrae variable stars. Gaia Data Release 3 data were used to fit an isochrone by varying parameters such as distance, reddening, metallicity, and age. The estimates obtained for these parameters were within uncertainty of the corresponding literature values despite a large range of metallicities that gave an appropriate fit; however, a significantly different proper motion in Right Ascension was used to screen for cluster membership. In addition, the periods for three of the RR Lyrae stars—V8, V31, V54—were confirmed using phase dispersion minimization (string length and standard deviation methods) as well as the Lomb-Scargle method. The colors of three RR Lyrae stars were also investigated through color analysis using data in the Johnson-Cousins V and Sloan Digital Sky Survey I-prime filters. ASAS-SN Sky Patrol data were used to determine if two select stars, V8 and V31, were undergoing period evolution. Because of inconclusive data, further investigation is suggested. Finally, the period-luminosity-metallicity (PLM) relationship was applied to recompute the distance to the cluster. The average derived PLM distance of 7.1 kpcs was a close match to previous distance estimates from the literature.

1. Introduction

1.1. Globular clusters and variable stars

M13 (NGC 6205), or the Hercules Globular Cluster, is located in the constellation Hercules in the galactic halo of the Milky Way. With an apparent magnitude of 5.8, M13 is one of the brighter globular clusters (GCs) as visible from Earth. Since all the stars in a cluster are of similar age and composition and are in the same location, isochrone fittings based on color-magnitude diagrams (CMDs) are commonly used to infer properties of age, distance, reddening, and metallicity (Hamrick *et al.* 2021; Deras *et al.* 2023). M13 has an estimated age of 12.5 Gyr (billion years) and an estimated distance of 7.3 kpc from Earth (Kumar *et al.* 2023; Gontcharov *et al.* 2020). Previous estimates of metallicity and reddening for M13 include [Fe/H] = –1.58 ± 0.04 and E(B–V) = 0.04 ± 0.01 (Carretta *et al.* 2009; Gontcharov *et al.* 2020). There are slight differences present around these parameters, with other research citing an age of 12.9 Gyr, a metallicity of [Fe/H] = –1.55, and reddening of E(B–V) = 0.02 (Denissenkov *et al.* 2017; Schlegel *et al.* 1998). Given the current variability in distance, metallicity, and reddening, an objective of this paper is both to evaluate the characteristics of M13 and derive distance from the period-luminosity-metallicity relationship with our periods of RR Lyrae stars.

RR Lyrae variable stars, which are commonly found in GCs, exhibit period-luminosity-metallicity relationships that can inform the investigation of the cosmic distance ladder, chemical abundances in our galaxy, and theoretical modeling of evolution and hydrodynamics within stellar structure (Lub 1978). Along with Cepheids and delta Scuti variables, RR Lyrae stars display pulsations driven by instability within the ionized He II convection zone, causing the stars to expand outward and then contract due to gravity (Shore *et al.* 2003). The variations set forth by this cycle are observed through changes in apparent magnitude, as seen through light curves.

Because of their relation to metallicity, RR Lyrae periods can serve as a marker in Oosterhoff's dichotomy to classify Milky Way globular clusters. Because of its preponderance of RRC-type variables, M13 is currently categorized as Oosterhoff group II (Kopacki *et al.* 2003). Metal-poor ([Fe/H] < –1.5) globular clusters that possess RRAB RR Lyrae stars with periods longer than 0.65 day are also classified as Oosterhoff group II, while metal-rich GCs whose RRAB stars have periods of approximately 0.55 day are part of Oosterhoff group I (Lee and Jang 2021). While the origin of the Oosterhoff dichotomy remains unclear (Kuehn *et al.* 2013), it has implications for both the formation of the Galactic halo and the evolution of the Milky Way (Kunder and Chaboyer 2009).

The RR Lyrae variables within M13 are documented in Clement's catalog (Clement *et al.* 2001). Though RRAB variables are often observed in globular clusters, M13 is thought to contain only one RRAB-type pulsator, while the rest are classified as RRC-type pulsators (Denissenkov *et al.* 2017).

RRAB pulsators, being the most common subclass of RR Lyrae variables, pulsate in a fundamental mode while RRC stars have rounded sinusoidal maxima (Percy and Tan 2013). RRC stars are also more likely to be found on the blue side of the instability strip on the HR diagram, intersecting the horizontal branch. RR Lyrae variables in M13 have been previously suggested to harbor potentially undetected companion stars or to exhibit the Blazhko effect, which causes a variation in their periods and amplitudes (Gillet 2013). Furthermore, V36 is a well-known multi-frequency or double mode pulsator (RRd), while recent measurements have suggested that V31 may be in that category as well (Clement *et al.* 2001; Deras *et al.* 2019). Because of the RR Lyrae complexity and importance within M13, we sought to either substantiate or update previous period measurements and investigate period variation or evolution.

2. Procedure

2.1. Target selection

M13 was chosen as a candidate for study because of its visibility in early spring as well as its preponderance of RR Lyrae stars. Ten RR Lyrae stars in M13 were selected from Clement's catalog[1] for further investigation (Clement *et al.* 2001). Out of the ten initially targeted RR Lyrae stars, only three produced resolvable light curves, likely due to their positions near the cluster periphery: V8 (V1550 Her), V31 (V1575 Her), and V54 (V1585 Her).

Potential comparison stars were queried using the AAVSO variable star plotter (VSP; AAVSO 2023), with a field of view of 30 arcminutes (0.5 degree) and a maximum numerical magnitude limit of 14.5. Stars 000-BNX-822 and 000-BNX-823 were chosen initially because of their being relatively close in magnitude to the RR Lyrae target stars. However, the photometry produced with this calibration caused the mean magnitudes in both the V and Ip filters to differ considerably from the averages reported by Deras *et al.* (2019). The comparison stars were changed to S2 and S3 from Stetson's 2000 catalog (Stetson 2000), which reduced differences in photometry in comparison to Deras'. Both sets of comparison stars are referenced in Table 1. Target RR Lyrae stars and the comparison stars used for this study are shown in Figure 1. A more comprehensive finder chart for this cluster exists in Deras *et al.* (2019).

2.2. Instruments used

The instruments used for the measurements in this paper were the Las Cumbres Observatory's 40-centimeter telescopes. These telescopes are equipped with several filters and an SBIG STL-6303 CCD camera. The Las Cumbres Observatory has ten 40-centimeter telescopes located in several places across the world, but the images analyzed here are from the Haleakala, Hawaii, USA, Tenerife, Spain, and Fort Davis, Texas, USA sites. Combining the telescope and camera gives a FOV of $0.32° \times 0.49°$ with a resolution of 0.57" per pixel. The filters used for the measurements made in this paper are the Johnson V filter and the Sloan Digital Sky Survey i' (i-prime, Ip), g' (g-prime, Gp), and r' (r-prime, Rp) filters (Bessel 1990; Fukugita *et al.* 1996).

Table 1. AAVSO Variable Star Plotter (VSP) comparison stars (Henden *et al.* 2016) and Stetson (2000) comparison stars.

AUID/Identifier	*R.A.* h m s	*Dec.* ° ′ ″	*V-mag*	*Ip-mag*
00-BNX-822	16 41 14.28	36 33 23.8	12.886	12.554
00-BNX-823	16 41 06.50	36 28 13.7	13.325	12.513
S2	16 41 15.10	36 23 53.9	14.617	13.650
S3	16 41 15.25	36 23 16.2	15.075	14.957

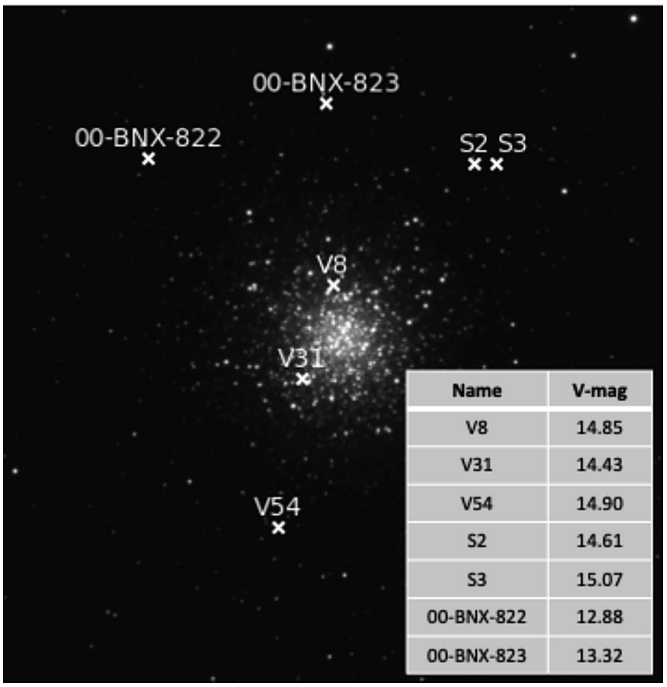

Figure 1. Locations of the target and comparison stars.

2.3. Exposure time

Exposure times are listed in Table 2. The exposure time was increased by 50 seconds for each filter following the 2/19/2023 measurement due to low ADU counts for the individual RR Lyrae stars. Using 10 random images in the Ip and V filters and averaging the values, the FWHM was measured for 2.00" for the V filter and 2.6" for the Ip filter.

2.4. Isochrone fitting

Gaia Data Release 3 (DR3) (Gaia Collaboration *et al.* 2016, 2018, 2023) provides a comprehensive set of data for the stars within the M13 cluster, which makes it highly useful for checking and refining known parameters of the cluster through isochrone fitting.

The isochrone model we used is part of the Cluster Pro Plus which is part of the Afterglow suite (Reichart 2021). The tool employs the PARSEC evolutionary tracks described in Nguyen *et al.* (2022), Marigo *et al.* (2013), and Pastorelli (2019, 2020). The photometric system is UBVRIJHK (Maíz Apellániz 2006; Bessell 1990) with bolometric corrections from Bohlin *et al.* (2020). Circumstellar dust is modeled using the scaling relations in Marigo *et al.* (2008) with 60% Silicate +

[1] https://www.astro.utoronto.ca/~cclement/cat/C1639p365

Table 2. Exposure times used.

Date (2023) (m/y)	*Filter*	*Exposure Time (sec)*	*No. of Images Returned*
02/17; 02/19	V	150	30
02/17; 02/19	IP	110	30
02/24; 02/25; 02/26; 03/01	V	200	55
02/24; 02/25; 02/26; 03/01	IP	160	53
03/03; 03/04; 03/17; 03/25; 04/17	V	200	57
03/03; 03/04; 03/17; 03/25; 04/17	IP	160	57

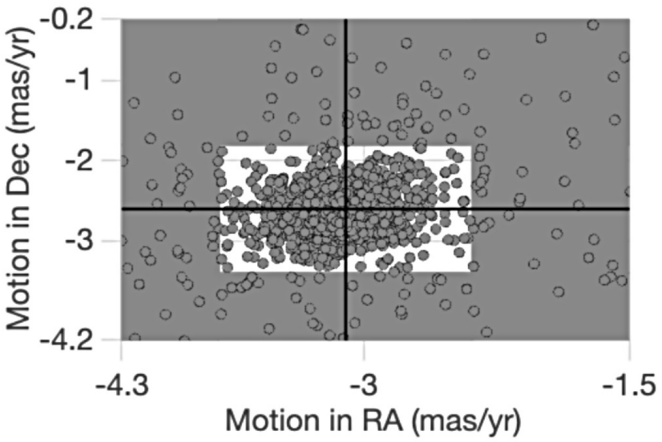

Figure 2. Proper motion graph for M13, using Gaia DR3 data, from the Skynet plotting tool.

40% AlOx for M stars and 85% AMC + 15% SiC for C stars as in Groenewegen (2006). Total extinction AV is set to 0.0 mag, using extinction coefficients computed star-by-star (except for the OBC case, which uses constant coefficients). The initial mass function for single stars used to compute stellar occupation along the isochrones comes from Kroupa (2001, 2002). An extinction curve was adopted from Cardelli *et al.* (1989) and O'Donnell (1994), with RV = 3.1, and is used for calibration of the reddening parameter.

Before fitting the isochrone parameters, Gaia DR3 stars were screened for cluster membership by examining Skynet's plot of each star's proper motion in R.A. and Dec. relative to the average proper motion of stars in the field as seen in Figure 2. All stars whose proper motions were significantly different, visually, from the average values were excluded from the isochrone (as seen in Figure 2).

Table 3. Number of images in which each star was resolvable on Our Solar Siblings' PSX photometry in the Ip and V filter.

Star	*Ip-filter Images*	*V-filter images*
V8	137	138
V31	141	141
V54	146	149

2.5. Light curve period procedure

Observation of the light intensity from RR Lyrae stars can be accumulated in a time series, plotted, and analyzed. Images were photometered by the Our Solar Siblings (OSS) pipeline (Fitzgerald 2018) which performs six different batch photometry algorithms. For purposes of this study, the OSS psx algorithm was used because it is a point spread function method and therefore most appropriate for this crowded field. The numbers of usable images in which each of the RR Lyrae stars was found for the Ip and V filters are shown in Table 4. The instrumental magnitude of each star was calibrated in order to make magnitude calculations standardized among other observations. Instrumental magnitudes (denoted as m) for the RR Lyrae and comparison stars were determined using the following formula, where F represents the flux:

$$m = (-2.5 \log_{10} (F)) \quad (1)$$

Then, the known magnitude of each comparison star in the V and Ip filter was subtracted from their respective instrumental magnitudes to obtain a specific calibration factor for each image. The instrumental magnitude of the RR Lyrae star was then found from the flux in the image, and adjusted by the calibration factor. Finally, the data were folded over the best period to create a plot of magnitude against phase.

Three methods of finding the best period were used and compared in this study. Two of these are phase dispersion

Table 4. Literature values and data obtained from the isochrone.

Parameter	*Characteristics from previous papers*	*Reference*	*Characteristics from fitted isochrone*
[Fe/H]	–1.58 ± 0.04 –1.55 –1.58 ± 0.09	Carretta *et al.* (2019) Denissenkov *et al.* (2017) Deras *et al.* (2019)	–1.58 (–1.38 [M/H])
E(B–V)	0.04 ± 0.01 0.02	Gontcharov *et al.* (2020) Denissenkov *et al.* (2017)	0.02
Distance (pc)	7399.8	Gontcharov *et al.* (2020)	7082.5
Log Age (years)	10.10 10.11	Kumar *et al.* (2023) Denissenkov *et al.* (2017)	10.04
Proper Motion (mas/year)	(–1.49 ± 0.36, –3.06 ± 0.35) (–1.1 ± 0.51, –2.3 ± 0.54)	Chen *et al.* (2002) Navin *et al.* (2016)	(–3.1 ± 0.7, –2.6 ± 0.8)

minimization (PDM) techniques: the string length period method (SLPM) and the standard deviation method, both of which we coded in Python. The string length method minimizes the total distance between the adjacent points in phase for the folded light curve (Altunin *et al.* 2020), while the standard deviation method minimizes the summed standard deviation of the fluxes for each of 10 bins (Stellingwerf 1978). For SLPM, periods were guessed in 0.0001-day (8.6-second) increments, and the corresponding string length was then graphed in a periodogram which is comparable to an inverted power spectrum (Bansal *et al.* 2022). The third period folding method was the Lomb-Scargle method, performed through a time-series analysis Python notebook and Skynet plotting (Fitzpatrick *et al.* 2014; VanderPlas 2018). For this method, periods were also guessed in 0.0001-day increments from 0 to 1 days. The period that produced the lowest value for PDM or the highest statistical power for Lomb-Scargle was returned and used to fold the light curve.

Code relating to best-period finding techniques are available at: https://github.com/keptzin/lightcurves/tree/main .

3. Results

3.1. Isochrone analysis

We report M13's proper motion to be (–3.1 ± 0.7 mas/yr, –2.6 ± 0.8 mas/yr), which differs notably from previously reported values for the proper motion of this cluster, particularly right ascension proper motion. Chen *et al.* (2002) reports M13's proper motion to be (–1.49 ± 0.36 mas/yr, –3.06 ± 0.35 mas/yr), and Navin *et al.* (2016) reports (–1.1 ± 0.51 mas/yr, –2.3 ± 0.54 mas/yr).

After screening for cluster membership using proper motion, field stars with distances from the Earth incompatible with cluster membership were excluded. This was determined visually from referencing Figure 2. For the remaining stars, the literature values for age, metallicity, and reddening shown in Table 3 were used initially for isochrone alignment and then adjusted for visual improvement to the fit. Since Cluster Pro Plus utilizes [M/H] (ratio of metals to H), a conversion is required to derive [Fe/H] (Catelan *et al.* 2004):

$$[M/H] = [Fe/H] + \log(0.638 \times 10^{0.3} + 0.362) = [Fe/H] + 0.2 \quad (2)$$

Our resulting isochrone fit is shown in Figure 3. The plot on the left compares the difference between the absolute magnitude in the Gaia BP and G filters to the absolute magnitude in the Gaia G filter; on the right, a simultaneous fit is performed using the Gaia BP and RP filters.

Although our fit suggests an age of about 1.5 billion years less than previous estimates, this estimate has a high uncertainty because the corresponding change to the logarithm age of the cluster (0.06 or 0.07) has a minimal effect on the shape of the isochrone. The prominent blue tail visible on the horizontal branch of the cluster (particularly visible in the BP/RP comparison) has been noted in Deras *et al.* (2019). The relative rarity of blue stragglers past the main sequence turnoff point compared to other clusters such as M3 has been noted by Ferraro *et al.* (1997). The literature age of the cluster suggests that most of the stars on the horizontal branch are burning helium in their cores. Where the instability strip crosses the horizontal branch, some stars in the RR Lyrae phase, head towards white dwarf status. The PARSEC model does not trace the shape of the blue horizontal branch because it is explicitly designed to model "evolutionary phases from the pre-main-sequence to the first few thermal pulses on the asymptotic giant branch or central C exhaustion" (Nguyen *et al.* 2022). Overall, the isochrone fit matched previous estimates for age, reddening, and distance, and the metallicity estimate was similar to previous literature measurements given unit conversion from [M / H] to [Fe/H].

3.2. Light curves

The resulting light curves for V8, V31, and V54 in the V and Ip filters from the three methods and their corresponding periodograms are shown in Appendix A. SLPM tended to return a period that was around double the literature value, causing the light curve to display two pulses. While V8 did not have this issue, both V31 and V54 did. This happens because the method is sensitive to harmonics, resulting in a string length of double the period being similar to that of a single period. Lomb-Scargle

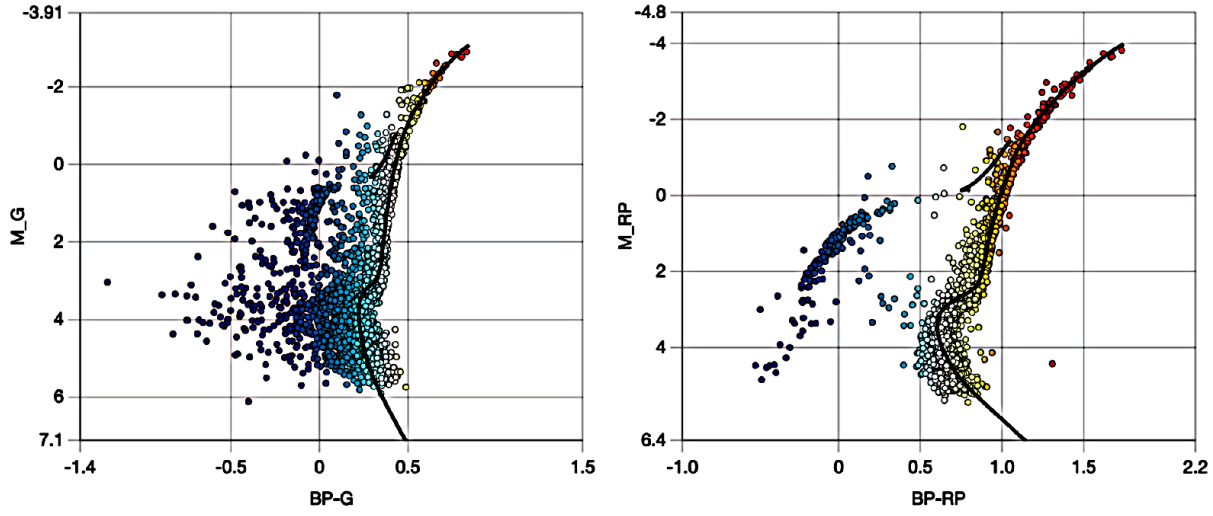

Figure 3. Isochrone fitting for Gaia DR3 data on M13 using different Gaia filters; –1.58 dex.

Table 5: Periods for V8, V31, and V54 found using different period folding methods.

RR Lyrae Star	*Deras (2019) Period*	*String-Length Period (Ip)*	*String-Length Period (V)*	*Standard Deviation Period (Ip)*	*Standard Deviation Period (V)*	*Lomb Scargle Period (Ip)*	*Lomb Scargle Period (V)*	*Classification*
V8	0.750303	0.749777	0.750208	0.750903	0.751203	0.750993	0.751132	RRAB
V31	0.329040	0.318348 (*)	0.420524 (*)	0.471440	0.286041	0.319057	0.319071	RRD
V54	0.295374	0.4541145	0.4547445 (*)	0.370974	0.295174	0.294869	0.294885	RRC

Note: (*) denotes SLPM value divided in half.

Table 6: Best periods for V8, V31, and V54, along with the method used.

RR Lyrae Star	*Best Period*	*Filter*	*Technique*
V8	0.750903 ± 0.0058	Ip	Standard Deviation
V31	0.319071 ± 0.0012	V	Lomb Scargle
V54	0.295174 ± 0.0019	V	Standard Deviation

also presents a weakness as it is optimized for sinusoids and RR Lyrae pulsations are sometimes not sinusoidal in shape. This method may also suppress harmonics, potentially interfering with the identification of eclipsing binaries. Table 5 summarizes the best period values from Clement's catalog, string length, standard deviation, and Lomb-Scargle methods.

As seen, the string length, standard deviation, and Lomb-Scargle methods had some variation within reported period, particularly the string length method. Generally, the V filter produced more distinct light curves. The standard deviation method in Ip presented the closest value to the Deras' previously found period. However, the range of periods that are suitable for V8 contributes towards a larger uncertainty for the best period. The Lomb-Scargle returned values for V31 closest to the reported Clement's catalog periods and the light curves produced with this method were also distinctly clearer, particularly in contrast to the light curves produced with SLMP. The identified period for V31 was considerably different from Deras' previous value, however, since V31 is identified as a RRd pulsator (double-mode), the secondary period may contribute to the scatter of the light curve. For V54, the standard deviation in the V filter produced both the closest value to the previous measurement and the clearest light curve.

The amplitude of oscillations approximately matched the corresponding values in the Clements catalog for all three variables. Ultimately, because the periods returned with all three methods were similar to those in Clement's catalog, confidence in these previously found measurements can be increased. Table 6 gives the resulting best periods for each RR Lyrae star.

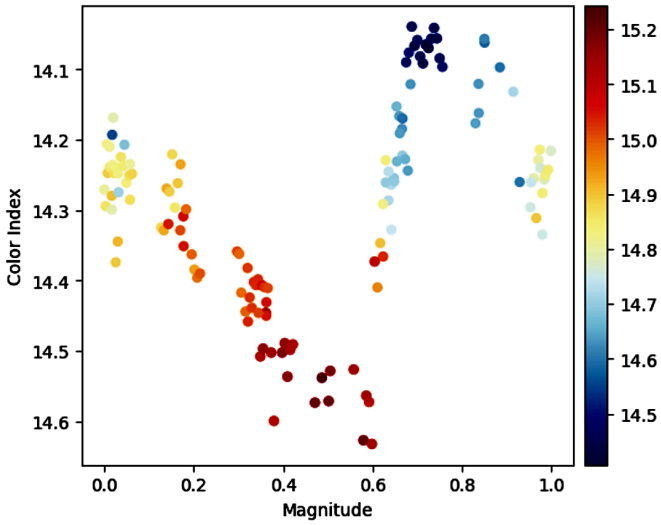

Figure 4. Photometric data of V8: magnitude indicated by y-axis, color index indicated by color bar (V–Ip magnitude). Period: 0.750903 day.

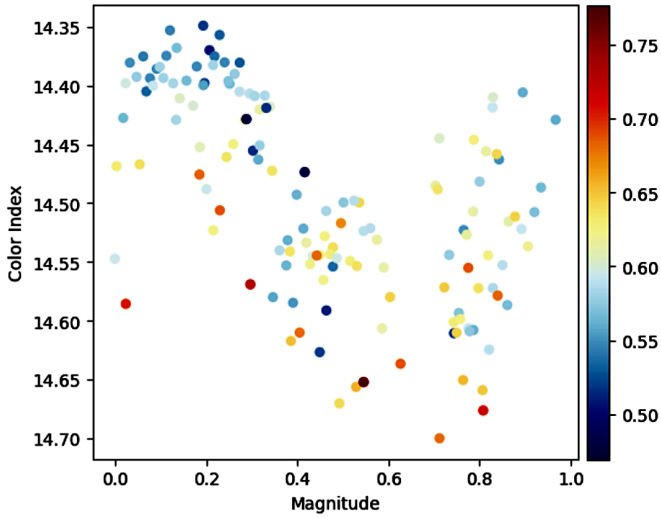

Figure 5. Photometric data of V31: magnitude indicated by y-axis, color index indicated by color bar (V–Ip magnitude). Period: 0.319071 day.

3.3. Color analysis

An analysis of the colors of the stars throughout the variation of their periods was conducted. The (V–Ip) color index at each date was computed by subtracting the calibrated V and Ip filter magnitudes of the stars from images whose timestamps were no more than 0.002 days (3 minutes) apart. In Figures 4 and 5, lower, more negative values correspond to a bluer, brighter star and the converse is true for a redder appearance. The resulting data were folded over the best period on the color data. Outliers (data points that were more than three standard deviations off of relative to their neighbors in the V magnitude or color) were removed for each star. As shown in Figures 4, 5, 6 for V8, V31, and V54 respectively, the stars become bluer as they become brighter. This phenomenon occurs because the luminosity of the star is proportional to temperature to the fourth power, while only being proportional to the radius squared. Therefore, as the star contracts and becomes bluer, its increase in temperature has a greater effect on luminosity, giving a greater brightness at the bluest points on the color diagram.

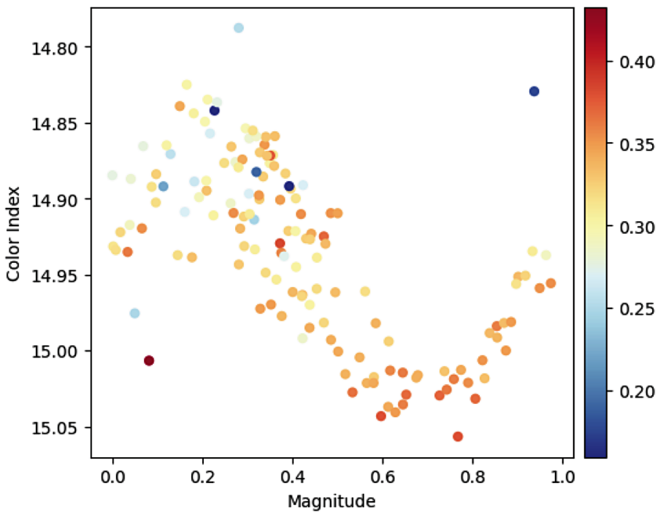

Figure 6. Photometric data of V54: magnitude indicated by y-axis, color index indicated by color bar (V–Ip magnitude). Period: 0.29514 day.

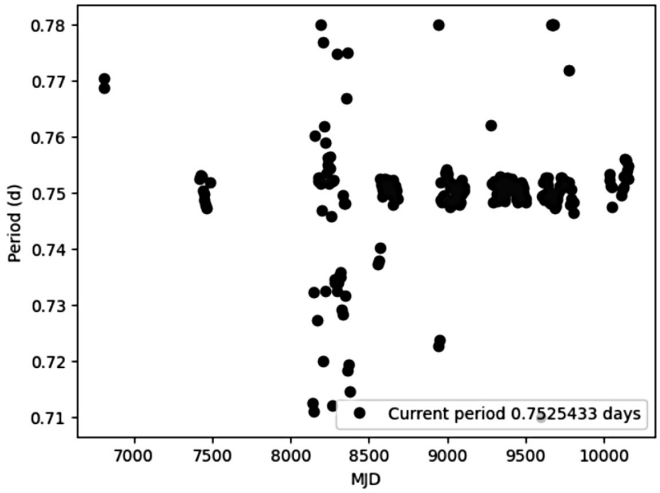

Figure 7. Period evolution plot for V8 using ASAS-SN data.

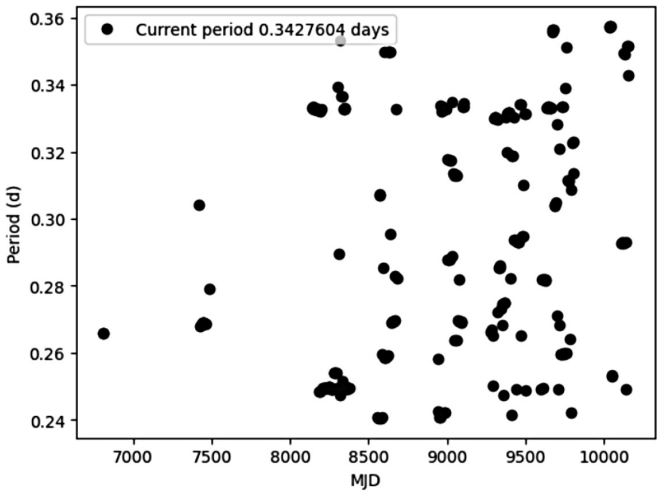

Figure 8. Period evolution plot for V31 using ASAS-SN data.

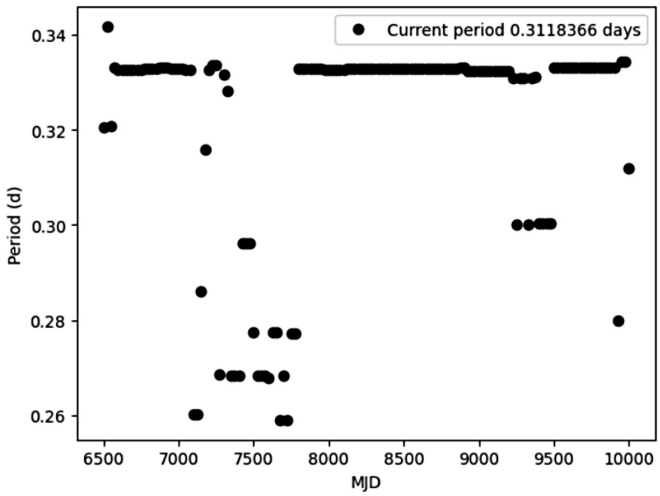

Figure 9. Larger bin period evolution plot for V31 using ASAS-SN data.

3.4. Period analysis and Blazhko effect

RR Lyrae stars are believed to be horizontal branch (HB) stars burning helium. Calculations from the rate of nuclear burning predict that until the end of the HB lifetime, the rate of period change would be small or near none. However, some RR Lyrae stars do exhibit period changes that are not in accordance with stellar evolution theory, such as pulsators that exhibit the Blazhko effect (Smith 2003). The stars V8 and V31 were examined for potential period evolution using data from the All-Sky Automated Survey for Supernovae (ASAS-SN) Sky-Patrol (Shappee *et al.* 2014; Kochanek *et al.* 2017). V54 was not analyzed because the overall ASAS-SN best period was in disagreement with our measured best period and the literature best period. Furthermore, the V54 light curves produced with our data are not sufficiently clean, and because of the short timescale during which our data were taken, the likely cause is measurement uncertainty rather than short-term period variation.

The GEOS database, which contains the data on maxima and T_0 to construct an O–C diagram, has only documented 17 variable stars in the Hercules constellation, none of which were our target stars. Therefore, we utilize a different method with ASAS-SN photometry within an 11-year timeframe. The period evolution algorithm separated the historical data into bins of a specific length and spacing in the time domain. The best period within each bin was determined via the Lomb-Scargle method (Janzen 2023). The bin size of 50 days and a midpoint spacing of 5 days between each midpoint were used to attempt to find shorter period changes. Figures 7 and 8 show the resulting graphs of the periods for V8 and V31, respectively, over 11 years.

As shown on the graph for V8, despite significant scatter in the data, the best period is consistently just over 0.75 day on average. The plot for V31 in Figure 8 shows significant variation happening across the range, with apparent rapid changes happening on a relatively periodic basis (every ~400 days or so), although this pattern is disturbed after about 9400 MJD. However, for both plots, the significant scatter can be

attributed to difficulty finding a period with insufficient data and the double-mode behavior present in an RRd star.

However, it should be noted that with 50-day bins, the number of data points decreases, resulting in the higher uncertainty evident in the graphs. Increasing the bin sizes to 500 or 1000 days can be helpful in significantly reducing this uncertainty. However, this also eliminates short-term period variation from the data set. To test more effectively over a longer term, an analysis of period variation was run with bin sizes of 500 days, and midpoint intervals of 25 days were run on V31. The resulting trend is shown in Figure 9.

The graph of period variation for V31 with larger bins shows a constant period except for the large outliers between 7000 and 8000 MJD. However, because the large bin sizes smooth over potential variations with periods of less than 200 days or so, *continuous* short-period changes cannot be ruled out or confirmed without both additional data and further study. This method cannot also yield conclusions about the Blazhko effects that can happen within as little as 40 days, because there would not necessarily be a period change, but rather a change to amplitude or phase (Smith *et al.* 2003; Lee and Schmidt 2001).

3.5. Period-Luminosity-Distance relationship

Like Cepheid variable stars, RR Lyrae stars can serve as standard candles to measure astronomical distances by finding the absolute magnitude of the star and comparing it to the observed apparent magnitude to derive distance. Unlike Cepheid variables, which have a tight period-luminosity relationship, the absolute magnitudes of RR Lyrae stars are typically obtained from the metallicity-luminosity relationship. In this case, another method is necessary, since the metallicities of the RR Lyrae stars within M13 have some uncertainty as described above. Like Cepheids, RR Lyrae stars exhibit a period-luminosity relationship, albeit one that is less precisely defined and not evident in all bands of light.

The relationship's ambiguity comes from RR Lyrae stars' positions on the horizontal branch. As the stars pulsate, they move through a much narrower range of luminosities and temperatures, necessitating the choice of a wavelength in which the range of absolute magnitudes over the course of a period is large (Catelan *et al.* 2004). The relationship is only tight in the near-infrared bands (IJHK), where "…the effects of luminosity and temperature conspire to produce tight relations…" (Catelan *et al.* 2004). Since there are larger amounts of scatter in the bluer bands, the relationship breaks down. Due to these conditions, the Ip filter was used for this analysis. The following equation was used for the PL relationship where MI is the absolute magnitude, P is the period, and Z is a variable based on metallicity. Since RRCs pulse in the first overtone, it is necessary to subtract 0.127 from log(P) to fundamentalize the period for V54 (Monson *et al.* 2017).

$$M_I = 0.4711 - 1.1318 \log(P) + 0.2053 \log(Z) \quad (3)$$

The following equation is needed to find log(Z). We will assume that [α/Fe] = 0.3 (Carney 1996).

$$\log(Z) = [Fe/H] + \log(0.638(10^{[\alpha/Fe]}) + 0.362) - 1.765 \quad (4)$$

The distance modulus equation was used to calculate distance.

$$d = 10^{0.2(m - M + 5 - 3.1E(B-V))} \quad (5)$$

Underestimating log(P) and overestimating log(Z) would result in the absolute magnitude becoming too large, propagating to lower the distance measurement (Latham *et al.* 2023). However, the effects of this are unlikely to be significant given our measurements of period and metallicity corresponding with previous measurements. Using the Ip-filter periods found from the Lomb-Scargle method, the metallicity, and E(B–V) of the cluster found from our fitted isochrone results in a distance greater than the previously estimated one. The closest results to previous measurements may be seen in Table 7. The average distance from our period luminosity calculation was 7114.39 pc in comparison to our isochrone fit of 7082 pc (23,100 ly). This is reasonably close to the previous literature estimates of 7300 pc (Kumar *et al.* 2023; Gontcharov *et al.* 2020) and 7100 pc (Deras *et al.* 2019).

4. Conclusions

We confirm the periods of three known RR Lyrae variable stars in M13 (V8, V54, and V31) with the string length, Lomb-Scargle, and standard deviation methods, and determine that they are bluest during the brightest parts of their phase. Our fitted isochrone with Gaia DR3 data suggests that updates to the previous literature values for proper motion in Right Ascension may be appropriate. Period investigation with ASAS-SN data indicates that period evolution of V8 and V31 is unlikely, but because of measurement uncertainty and difficulty finding the best period over time, it is suggested that further examination is needed to shed light on these candidates. Finally, we investigate the period-luminosity-distance relationship and estimate the distance of M13 using its RR Lyrae stars.

Table 7. Values and returns of the PL calculations.

Target Star	*Median apparent magnitude in Ip from OSS PSX photometry*	*Calculated absolute magnitude*	*Best period*	*Distance (parsecs)*	*[Fe/H] (dex)*	*E(B–V)*
V8	14.619	≈ –0.0309	0.750903	≈ 8271.71	–1.58	0.02
V31	14.242	≈ 0.3897	0.319071	≈ 5728.73	–1.58	0.02
V54 (*)	14.963	≈ 0.5717	0.295174	≈ 7342.73	–1.58	0.02

Note: (*) denotes that the period was fundamentalized.

5. Acknowledgements

This work makes use of observations taken by the 0.4-m telescopes of Las Cumbres Observatory Global Telescope Network located in Haleakala, Hawaii, USA, Tenerife, Spain, and Fort Davis, Texas, USA.

This research was made possible by Astrometry.net, the AstroImageJ software which was written by Karen Collins and John Kielkopf, PixInsight developed by Pleiades Astrophoto, and Afterglow, a Skynet software. This paper contains plots constructed using PixInsight software. This research also made use of the Skynet plotting tool for isochrones and period search in the Lomb-Scargle method.

This work has also made use of data from the European Space Agency (ESA) mission Gaia (https://www.cosmos.esa.int/gaia), processed by the Gaia Data Processing and Analysis Consortium (DPAC; https://www.cosmos.esa.int/web/gaia/dpac/consortium). Funding for the DPAC has been provided by national institutions, in particular, the institutions participating in the Gaia Multilateral Agreement.

We acknowledge with thanks the variable star observations from the AAVSO International Database (Kloppenborg 2023) contributed by observers worldwide and used in this research.

The authors also thank the anonymous referee and the editor for their comments and constructive feedback which greatly improved this paper.

References

AAVSO. 2023, Variable Star Plotter (VSP; https://www.aavso.org/apps/vsp/).

Altunin, Caputo, R., and Tock, K. 2020, *Astron. Theory, Obs. Methods*, **1**, 1.

Bansal, A., Hamrick, P., and Tock, K. 2022, *J. Amer. Assoc. Var. Star Obs.*, **50**, 34.

Bessell, M. S. 1990, *Publ. Astron. Soc. Pacific*, **102**, 1181.

Bohlin R. C., Hubeny I., and Rauch T. 2020, *Astron. J.*, **160**, 21.

Cardelli J. A., Clayton G. C., and Mathis J. S. 1989, *Astrophys. J.*, **345**, 245.

Carney, B. W. 1996, *Publ. Astron. Soc. Pacific*, **108**, 900.

Carretta, E. Bragaglia, A., Gratton, R., D'Orazi, V., and Lucatello, S. 2009, *Astron. Astrophys.*, **508**, 695.

Catelan, M., Pritzl, B. J., and Smith, H. A. 2004, *Astrophys. J., Suppl. Ser.*, **154**, 633.

Chen, L., Wang, J. J., and Zhao, J. L. 2002, in *Extragalactic Star Clusters*, eds. D. Geisler, E. K. Grebel, D. Minniti, IAU Symp. 207, Astronomical Society of the Pacific, San Francisco, 119.

Clement, C. M., *et al.* 2001, *Astron. J.*, **122**, 2587.

Denissenkov, P. A., VandenBerg, D. A., Kopacki, G., and Ferguson, J. W. 2017, *Astrophys. J.*, **849**, 159.

Deras, D., Arellano Ferro, A., Lázaro, C., Bustos Fierro, I. H., Calderón, J. H., Muneer, S., and Giridhar, S. 2019, *Mon. Not. Roy. Astron. Soc.*, **486**, 27.

Deras, D. *et al.* 2023, *Astrophys. J.*, **942**, 104.

Ferraro, F. R., Paltrinieri, B., Fusi Pecci, F., Cacciari, C., Dorman, B., and Rood, R. T. 1997, *Astropohys. J.*, **484**, L145.

Fitzgerald, M. T. 2018, *Robotic Telesc. Student Res. Education Proc.*, **1**, 347.

Fitzpatrick, M. J., *et al.* 2014, *Proc. SPIE*, **914**, 91491.

Fukugita, M., Ichikawa, T., Gunn, J. E., Doi, M., Shimasaku, K., and Schneider, D. P. 1996, *Astron. J.*, **111**, 1748.

Gaia Collaboration, Babusiaux, C., *et al*. 2018, *Astron. Astrophys.*, **616A**, 10.

Gaia Collaboration, Prusti, T., *et al.* 2016, *Astron. Astrophys.*, **595A**, 1.

Gaia Collaboration, Vallenari, A. G. A., *et al.* 2023, *Astron. Astrophys.*, **674**, 1.

Gillet. D. 2013, *Astron. Astrophys.*, **554A**, 46.

Gontcharov, G. A., Khovritchev, M. Y., and Mosenkov, A. V. 2020, *Mon. Not. Roy. Astron. Soc.*, **497**, 3674.

Groenewegen M. A. T. 2006, *Astron. Astrophys.*, **448**, 181.

Hamrick, P., Bansal, A., and Tock, K. 2021, *J. Amer. Assoc. Var. Star Obs.*, **49**, 192.

Henden, A. A., Templeton, M., Terrell, D., Smith, T. C., Levine, S., and Welch, D. 2016, VizieR Online Data Catalog: AAVSO Photometric All Sky Survey (APASS) DR9, II/336.

Janzen, D. 2013, private communication.

Kloppenborg, B. 2023, Observations from the AAVSO International Database (https://www.aavso.org/databases).

Kochanek, C. S., *et al.* 2017, *Publ. Astron. Soc. Pacific*, **129**, 104502.

Kopacki, G., Kołaczkowski, Z., and Pigulski, A. 2003, *Astron. Astrophys.*, **398**, 541.

Kroupa, P. 2001, *Mon. Not. Roy. Astron. Soc.*, **322**, 231.

Kroupa, P. 2002, *Mon. Not. Roy. Astron. Soc.*, **330**, 707.

Kuehn, C., *et al.* 2013, *Astron. J.*, **145**, 160.

Kumar, R., Pradhan, A. C., Sahu, S., Subramaniam, A., Piridi, S., Cassisi, S., and Ojha, D. K. 2023, *Mon. Not. Roy. Astron. Soc.*, **522**, 847.

Kunder, A., and Chaboyer, B. 2009, *Astron. J.*, **138**, 1284.

Latham, C., Kamenetzky, J., and Fitzgerald, M. T. 2023, *Res, Notes AAS*, **7**, 68.

Lee, K. M., and Schmidt, E. G. 2001, *Publ. Astron. Soc. Pacific*, **113**, 1140.

Lee, Y.-W., and Jang, S. 2021, in *RR Lyrae/Cepheid 2019: Frontiers of Classical Pulsators*, eds. K. Kinemuchi, C. Lovekin, H. Neilson, K. Vivas, ASP Conf. Ser. 529, Astronomical Society of the Pacific, San Francisco, 169.

Lub, J. 1978, *Messenger*, **13**, 15.

Maíz Apellániz, J. 2006, *Astron. J.*, **131**, 1184.

Marigo, P., Bressan, A., Nanni, A., Girardi, L., and Pumo, M. L. 2013, *Mon. Not. Roy. Astron. Soc.*, **434**, 488.

Marigo, P., Girardi, L., Bressan, A., Groenewegen, M. A. T., Silva, L., and Granato, G. L. 2008, *Astron. Astrophys.*, **482**, 883.

Monson, A. J., *et al.* 2017, *Astron. J.*, **153**, 96.

Navin, C. A., Martell, S. L., and Zucker, D. B. 2016, *Astrophys. J.*, **829**, 123.

Nguyen, C. T., *et al.* 2022, *Astron. Astrophys.*, **665A**, 126.

O'Donnell, J. E. 1994, *Astrophys. J.*, **422**, 158.

Pastorelli, G., *et al.* 2019, *Mon. Not. Roy. Astron. Soc.*, **485**, 5666.

Pastorelli, G., *et al.* 2020, *Mon. Not. Roy. Astron. Soc.*, **498**, 3283.

Percy, J. R., and Tan, P. J. 2013, *J. Amer. Assoc. Var. Star Obs.*, **41**, 75.

Reichart, D. E. 2021, *Phys. Teacher*, **59**, 728.
Schlegel, D. J., Finkbeiner, D. P., and Davis, M. 1998, *Astrophys. J.*, **500**, 525.
Shappee, B. J., *et al.* 2014, *Astrophys. J.*, **788**, 48.
Shore, S. N., *et al.* 2003, in *Encyclopedia of Physical Science and Technology*, 3rd ed., ed. R. A. Meyers, Academic Press, San Diego, 737.
Smith, H. A. 2003, arXiv:1310.0533.
Smith, H. A., *et al.* 2003, *Publ. Astron. Soc. Pacific*, **115**, 43.
Stellingwerf, R. F. 1978, *Astrophys. J.*, **224**, 953.
Stetson, P. B. 2000, *Publ. Astron. Soc. Pacific*, **112**, 925.
VandenBerg, D. A., Brogaard, K., Leaman, R., and Casagrande, L. 2013, *Astrophys. J.*, **775**, 134.
VanderPlas, J. T. 2018, *Astrophys. J., Suppl. Ser.*, **236**, 16.

Appendix A

Below are the light curves produced and corresponding periodograms with the string length method, standard deviation method, and Lomb-Scargle, respectively.

String-Length Method

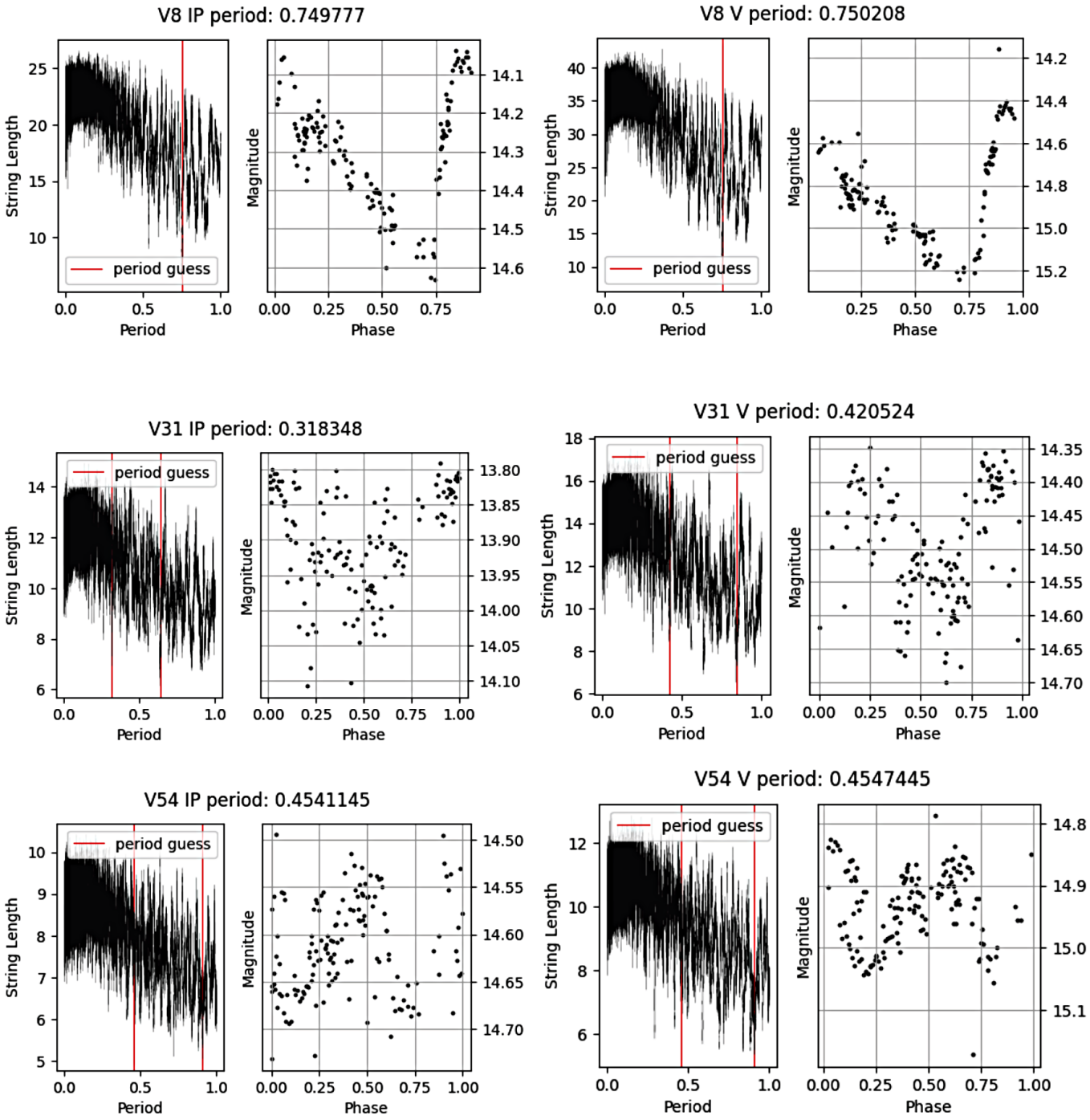

Standard Deviation Technique

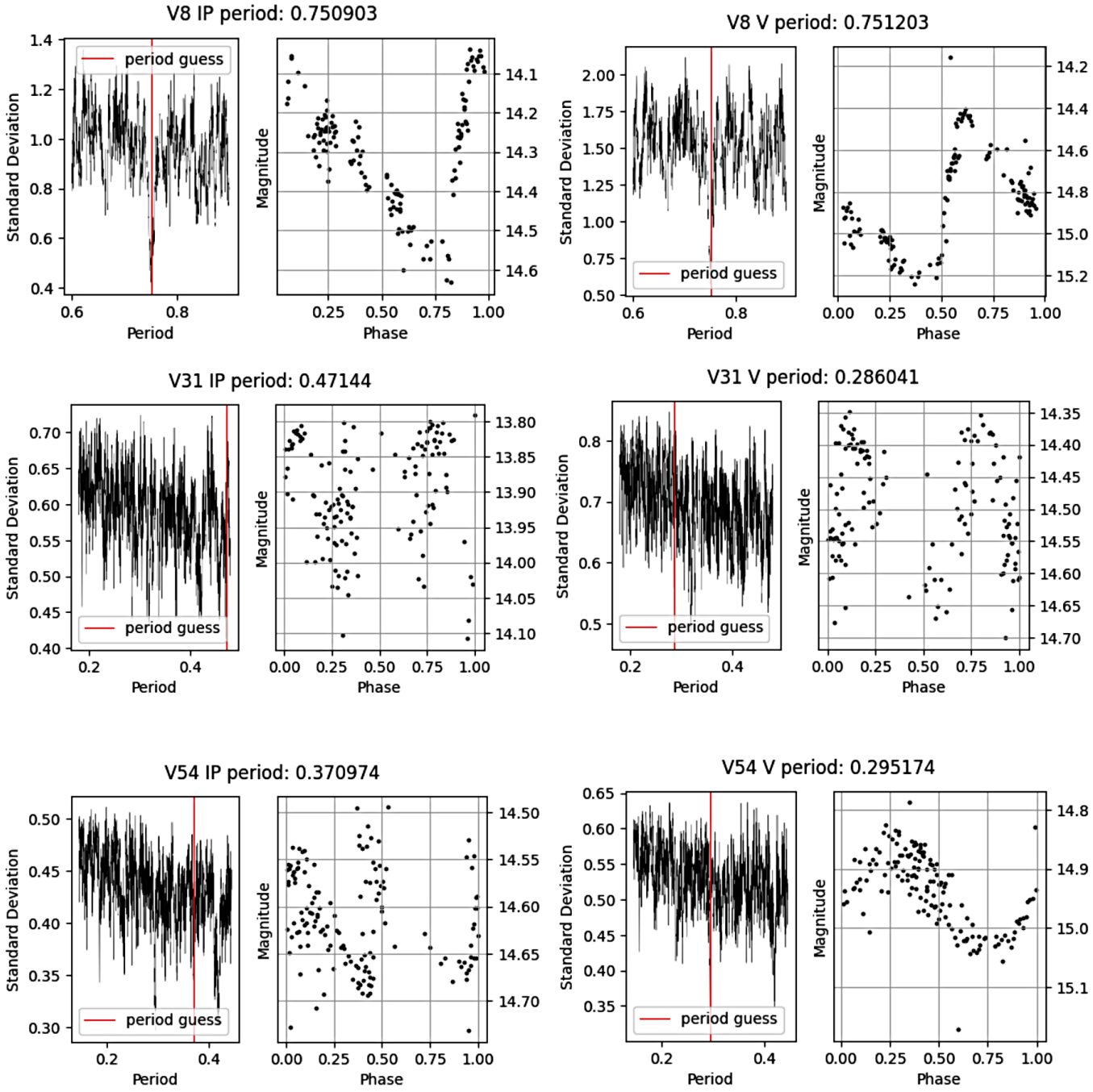

Lomb-Scargle Technique